



Intracellular pathway of halloysite nanotubes: potential application for antitumor drug delivery

Haoyang Liu¹ , Zhi-Gang Wang¹ , Shu-Lin Liu¹ , Xihui Yao¹ , Yun Chen¹ , Shirley Shen² , Yu Wu¹ , and Weiqun Tian^{1,*}

¹Department of Biomedical Engineering, School of Basic Medical Sciences, Wuhan University, Wuhan, China

²CSIRO Manufacturing, Clayton, Melbourne, VIC 3168, Australia

Received: 4 May 2018

Accepted: 2 August 2018

Published online:

10 August 2018

© Springer Science+Business Media, LLC, part of Springer Nature 2018

ABSTRACT

Natural halloysite nanotubes (HNTs), with nanotubular structure, are attracting considerable attention in recent years. The hollow tubular structure allows HNTs to play an important role in drug delivery system as drug carriers. However, the wide applications of HNTs in biomedicine have been hampered by the lack of sufficient intracellular researches so far. In this study, we systematically investigated the transport mechanisms of HNTs in A549 living cells. The colocalization and inhibition experiments illustrated FITC-labeled HNTs were readily internalized into cells by both clathrin- and caveolae-dependent endocytosis, and the transport pathway of HNTs is an actin- and microtubule-associated process via Golgi apparatus and lysosome. Meanwhile, the cell cycle assay clarified that HNTs can prompt the intracellular transportation of gemcitabine and enhance the gemcitabine concentration in A549 tumor cells. Such elucidation of intracellular transport pathway of HNTs offers insights into the site-specific delivery and cellular internalization of HNTs, which provide a reasonable guidance for the design of novel drug delivery system.

Introduction

Nanomaterial-based drug carriers have attracted considerable interest because they allow targeted delivery, efficient loading and controlled release of drugs. Especially, inorganic nanomaterials, such as carbon nanotubes, graphene oxides, gold nanoparticles and various inorganic nanoparticles [1–6], have brought many fascinating ideas and opportunities for disease diagnosis and treatment as novel drug

carriers. HNT is a kind of naturally deposited aluminosilicate ($\text{Al}_2\text{Si}_2\text{O}_5(\text{OH})_4 \cdot n\text{H}_2\text{O}$), similar to the chemical composition of kaolin [7–9]. HNTs have a predominantly hollow tubular structure in the sub-micrometer range, because the neighboring alumina and silica layers are curved and rolled up by water hydration [10, 11]. A key function for such a hollow cylindrical nanostructure is to serve as a good cargo carrier by entrapping a range of materials in the inner lumen with controlled releases [11–16]. HNTs as natural nanotubular products are cheap and readily

Address correspondence to E-mail: tian_weiqun@whu.edu.cn

available and have a very minimal influence on the environment compared to the above-mentioned nanoparticles. Especially, the chemical properties of the HNTs are similar to the properties of Al_2O_3 on inner surface and are associated with the properties of SiO_2 on the outer surface [8, 17], which allow to modify the inner and outer walls separately for various possibilities.

Recently, HNTs as delivery systems for drug molecules into cells and living tissues have obtained more and more attention [18–20]. HNTs have been reported to have good biocompatibility and safety profile following the cellular internalization [5, 9]. With the aid of confocal microscopy, intracellular accumulation of HNTs was found with perinuclear localization [9, 21]. Although HNTs could be used as a good cargo nanocarrier [22–25], many fundamental and practical issues still remain not addressed. Intracellular studies of CNTs, which have a similar tubular structure to HNTs, have been extensively explored by fluorescence labeling techniques [26, 27]. However, how HNTs are internalized into living cells and what is the transport pathway of HNTs in living cells remain questions so far.

Gemcitabine (2',2'-difluorocytidine monohydrochloride), a pyrimidine analog, exhibits the potent activity for the treatment of patients with pancreatic cancer [28] and non-small cell lung cancer (NSCLC) [29]. These clinical data suggest the promising therapeutic effects of gemcitabine in the treatment of pancreatic cancer and NSCLC. However, the delivery efficiency and targeting remain underdeveloped.

In this work, to probe the cellular uptake of HNTs and to determine what happens to the particles once they are inside the cell are mainly focused. FITC was initially utilized to label APTES-modified HNTs, and then the internalized pathway of HNTs in living cells has been systematically studied with the aid of a confocal microscopy. FITC-labeled HNTs appeared in the living cells, and the distribution of HNTs inside cells is also shown. By different endocytosis-inhibiting experiments, the endocytosis pathways and intracellular fate of HNTs have also been detected. Besides, HNTs have been proved to contribute to the transmembrane delivery of gemcitabine by cell cycle assay. Therefore, the results provide a deeper insight into the intracellular transport pathway of HNTs.

Materials and methods

Materials

HNTs were purchased from Jin Yang Guang Ceramic Co. Ltd (Zhengzhou, China). Fluorescein isothiocyanate isomer I (FITC), aminopropyl-triethoxysilane (APTES), cytochalasin D, filipin, nocodazole and chlorpromazine were obtained from Sigma-Aldrich (Shanghai, China). Hoechst 33342, DiD, LysoTracker Red, Golgi-Tracker Red and cell cycle assay kit were purchased from Beyotime Biotechnology Co. Ltd (Nantong, China). Fetal bovine serum (FBS), DMEM, trypsin/EDTA and penicillin–streptomycin were purchased from Hyclone Co. (South Logan, UT). Purified deionized water prepared by Milli-Q system (Millipore Co., Billerica, MA, USA) was used to prepare all of the solutions. Gemcitabine was purchased from Haosen Pharmacy Co. Ltd (Jiangsu, China) and was used as received.

Cell culture

Human lung cancer cells (A549 cells)/human lung fibroblasts (MRC-5 cells) were maintained in DMEM supplemented with 10% FBS, penicillin (100 mg/mL) and streptomycin (100 $\mu\text{g}/\text{mL}$) in a humidified 5% CO_2 atmosphere at 37 °C. For fluorescence imaging, the cells were cultured on the glass-bottomed 35-mm Petri dishes and allowed to grow until a confluence of 70–80%. Before the uptake studies, cells were washed twice with Tyrode's plus buffer to remove the remanent growth medium.

HNTs separation

HNTs firstly suspended in buffer solution by ultrasonic dispersion and then centrifuged 5 min at the speed of 3000 rpm. The HNTs in the supernatant were centrifuged 10 min at the speed of 9000 rpm and freeze-dried overnight for further usage. By virtue of this procedure, we can obtain the relatively even distribution of the size of HNTs.

Fluorescence labeling

To perform fluorescence imaging experiments, a classical method to obtain FITC-labeled HNTs was used [9, 30]. In brief, the surface of HNTs was modified with APTES and then FITC was added to obtain

FITC-labeled HNTs. The detailed procedure is as follows. First, HNTs were modified with APTES [30, 31]. APTES (500 μL) was dissolved in 50 mL of ethanol initially and mixed with 0.5 g of HNTs. After being dispersed ultrasonically for 30 min, the suspension was then refluxed with constant stirring at 80 $^{\circ}\text{C}$ for 20 h. To remove the excess of organosilane, the resultant mixture was washed with fresh ethanol six times and dried overnight at 85 $^{\circ}\text{C}$. Then, the mixture was washed ten times with DI water, and the sample was freeze-dried overnight. Second, the amino-modified nanotubes were labeled with FITC. 3 mg of functionalized nanotubes were dispersed in 1.5 mL of 0.1 M carbonate buffer (pH 8.0). Then, 100 μL of 13 mM FITC solution was added. At room temperature, the mixture was reacted with constant stirring in a dark place for 2 days. The solution was then dialyzed to remove any un-reacted dyes and lyophilized overnight.

After 3 h incubation with FITC-labeled HNTs, the A549 cells were washed with fresh Tyrode's plus buffer and then incubated in Tyrode's plus buffer containing 5 mg/ml DiD and 5 mg/ml Hoechst 33342 for 30 min at 37 $^{\circ}\text{C}$ to label the cell membrane and nucleus for fluorescence imaging. Likewise, to label the Golgi apparatus and lysosome, the cells were incubated with 50 nM Golgi-Tracker Red and 50 nM LysoTracker Red in fresh culture medium for 30 min at 37 $^{\circ}\text{C}$, respectively.

Scanning electron microscopy (SEM) and transmission electron microscopy (TEM)

For SEM analysis, a drop of the halloysite suspension was applied to a metal wafer and dried at room temperature overnight. The measurements were conducted using a Quanta 200 FEG field emission scanning electron microscope (Bruker, Germany) at an operating voltage of 15.0 kV.

TEM images of HNTs were recorded with a Tecnai 12 transmission electron microscope (FEI, Eindhoven, the Netherlands) at an operating voltage of 120 kV. Images were recorded using a Megaview III CCD camera and analysis camera control software (Olympus). The samples were prepared by dropping a suspension of halloysite nanotubes onto carbon-coated 300-mesh copper grids and then allowing water to evaporate for analysis.

MTT assay

A549 cells were seeded in 96-well plates. After 24 h, they were exposed to 100- μL suspension of nano-materials, from 25 to 200 $\mu\text{g}/\text{mL}$ during 48 to 72 h. A control was a complete culture medium. After exposure, cultures were removed and 10 μL of 5 mg/mL MTT solution was aseptically added to each well. After 3 h at 37 $^{\circ}\text{C}$, medium was then replaced by 150 μL of dimethyl sulfoxide and mixed thoroughly to dissolve the formazan crystals. An absorbance at wavelength of 490 nm was measured with BioTek Elx800 UV-Vis spectrophotometer. The cell viability percentage was expressed by equation

$$\text{Cell viability} = (D_{\text{sample}}/D_{\text{control}}) \times 100\%,$$

where D_{sample} and D_{control} are the absorbance of the sample and the control.

Confocal microscopy

Fluorescence images were recorded with a spinning-disk confocal microscope (Andor Revolution XD), which is equipped with a CO_2 online culture system (INUBG2-PI), an EMCCD (Andor iXon DV885 K) and a 100 \times objective. For multi-color imaging, the 405 nm, 488 nm, 561 nm and 640 nm laser (DPSS, USA) were used to excite Hoechst 33342, FITC, LysoTracker Red/Golgi-Tracker Red and DiD, respectively. The fluorescence signals were separated using 447/60 nm, 525/50 nm, 617/73 nm and 685/40 nm (Chroma) emission filters and imaged alternately onto the EMCCD by separate channels.

Inhibition studies

To explore the internalization pathway of HNTs, the A549 cells were exposed in Tyrode's plus buffer with cytochalasin D (20 mM, to disrupt actin filaments), filipin (5 $\mu\text{g}/\text{mL}$, to inhibit the formation of caveolae), nocodazole (60 mM, to inhibit the formation of microtubules) and chlorpromazine (10 $\mu\text{g}/\text{mL}$, to inhibit the formation of clathrin vesicles) for 30 min, respectively, and then FITC-labeled HNTs were added for an additional 2 h. The cells were, then, washed twice with fresh Tyrode's plus buffer for fluorescence imaging.

Drug-loading procedure

For the encapsulation of gemcitabine, HNTs (20 mg), as dry powder, were added to an aqueous solution of gemcitabine (3 mL, 1 mg/mL) and stirred at 1000 rpm for 12 h at room temperature. Then, the solution was centrifuged at 9000 rpm and washed with distilled water three times. To evaluate the gemcitabine loading capacity, the residual gemcitabine content in the supernatant was collected and was measured by UV–Vis spectroscopy at the wavelength of 261 nm.

Cell cycle assay

A549/MRC-5 cells seeded on the 6-well plates were treated with pristine HNTs, gemcitabine and gemcitabine-loaded HNTs at 37 °C for 24 h. Cells treated with FBS-free culture medium served as control. At the end of incubation, adherent and non-adherent cells were trypsinized. Cells were collected by centrifugation at 1000 g for 5 min, washed twice with ice-cold PBS and then fixed with 70% cold ethanol and stored at 4 °C for 24 h. Cells were centrifuged again, washed with ice-cold PBS twice, incubated with RNase A (0.1 mg/mL) for 1 h at 37 °C and stained with propidium iodide (PI) (0.1 mg/mL) for 30 min in the dark. The DNA content was measured by flow cytometry (BD FACSCalibur, USA), and the percentage of cells in each phase of the cell cycle was evaluated using the Expo32v1.2 analysis software and MultiCycle for Windows 32-bit.

Results

Characterization of halloysite nanotubes

The structure of the nanotubes was characterized by scanning electron microscopy (SEM) and transmission electron microscope (TEM), respectively. HNTs have regular long shapes in the SEM image (Fig. 1a). TEM images further confirmed that the inner area of HNTs is hollow and open-ended (Fig. 1b). The diameter of HNTs is 32 ± 8 nm, and the length is 225 ± 117 nm (peak $\pm 1/2$ half-width) as shown in Fig. 1c. The dynamic light scattering (DLS) result shows that the hydrodynamic diameter of HNTs is around 332 ± 135 nm with good dispersity (Fig. S1).

MTT assay

The cytotoxicity profile of the HNTs was examined by MTT assay, where A549 cells were treated with either original HNTs or FITC-labeled HNTs (Fig. S2). For both original HNTs (Fig. S2a) and FITC-labeled HNTs (Fig. S2b), A549 cell viability was maintained at 70% up to a concentration of 75 $\mu\text{g/mL}$. It is demonstrated that FITC-labeled HNTs are almost as non-toxic to the cells as original HNTs in a low concentration. Thus, the experimental concentration of 10 $\mu\text{g/mL}$ was used throughout the study to ensure the nearly full viability of cells.

Distribution of FITC-labeled HNTs in living cells

Live A549 cells incubated with FITC-labeled HNTs were observed at the first time using a confocal microscope. Figure S3a shows an example of A549 cells treated with FITC-labeled HNTs. The fluorescence signal can be clearly observed inside the cells, and the outlines of cells are even displayed clearly. FITC-labeled HNTs can be seen to readily enter into the cells as the fluorescence signal shows. Those 12 Z-stacks of the cells were reconstructed in 3D surface plots (shown in Fig. S3a-right), further illustrating that FITC signals can indicate the existence of HNTs in the cells and the HNTs can be internalized into cells. Fig. S3b is a negative control (HNTs without FITC-labeled), where fluorescence signals could not be detected. However, it is reasonable that HNTs without FITC-labeled can enter into cells.

Then, the distribution of FITC-labeled HNTs in live A549 cells has been investigated. First, the cells were incubated with FITC-labeled HNTs, and then the membrane of the treated cells was labeled by DiD simultaneously (Fig. 2). Snapshots of different Z slices of the cells show that the FITC-labeled HNTs signals not only appeared inside the cells but also aggregated in a specific region of the cells (Fig. 2a). It indicates that the distribution of HNTs is heterogeneous in the cytoplasm. The orthogonal view of the cells shows the intracellular accumulation of the nanotube particles or agglomerates and further confirms the existence of HNTs inside the cell (Fig. 2b). Meanwhile, the nucleus of the treated cells was labeled by Hoechst 33342. It was found that FITC signals appeared in the perinuclear region of the cell nucleus, but were not observed in the cell nucleus

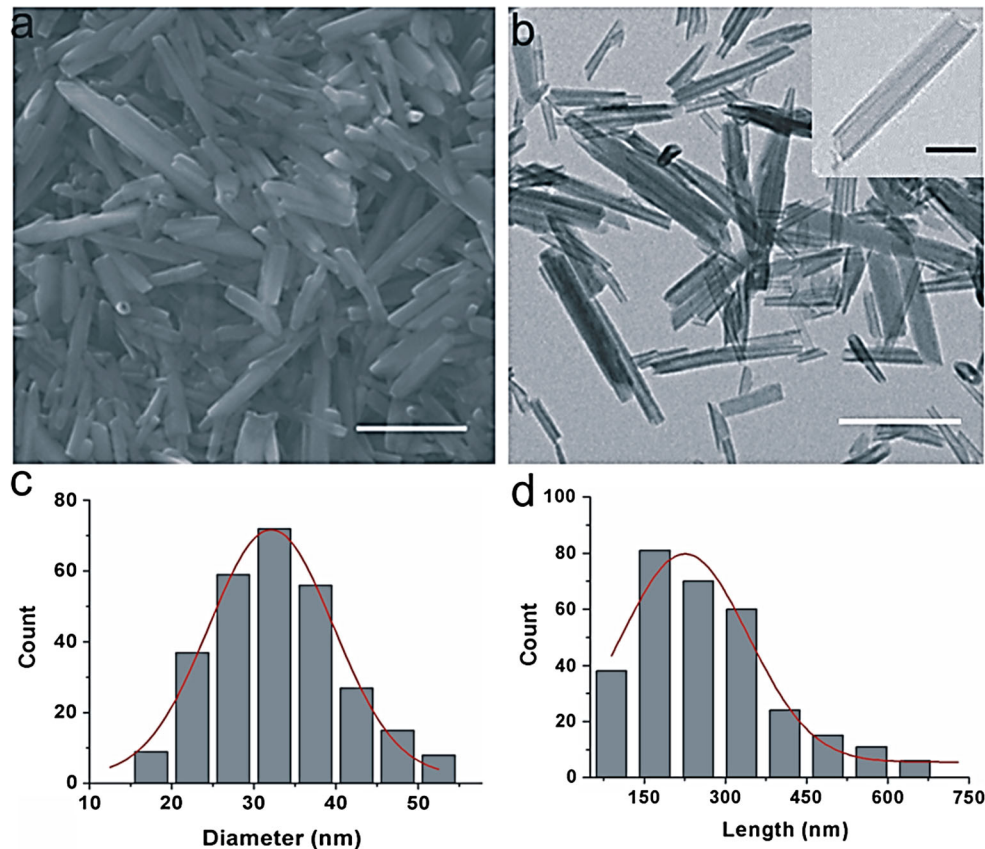


Figure 1 Characterization of original halloysite nanotubes (HNTs): **a** SEM image of halloysite nanotubes (scale bar: 500 nm). **b** TEM image of halloysite nanotubes (scale bar:

300 nm). The inset is the magnified TEM image of single nanotubes (scale bar is 50 nm). **c** and **d** histograms of the diameter and length of HNTs.

even at a prolonged incubation time. So the HNTs could not enter into the cell nucleus (Fig. 2c–e).

To further illustrate the distribution of HNTs near the cell nucleus, A549 cells were incubated with FITC-labeled HNTs and then stained with Golgi-Tracker Red (a Golgi apparatus dye) and LysoTracker Red (a lysosomal compartment dye), respectively. As shown in Fig. 3a, the HNTs signals are partially colocalized with the Golgi-Tracker Red signals, indicating that the HNTs are transported via Golgi apparatus in living cells. In the meanwhile, the HNTs signals are also colocalized with LysoTracker Red signals, suggesting that the HNTs are also transported into lysosomes in living cells (Fig. 3b). The line profiles of the cells revealed that most of the intensity peaks of FITC-labeled HNTs signals accompanied the appearance of those of labeled Golgi apparatus (Fig. 3c) and lysosome (Fig. 3d). It further confirms that HNTs have been transported via both of these organelles.

Intracellular transport pathway of HNTs

To date, several endocytic processes that enclose nanoparticles in membrane vesicles in an energy-dependent manner are identified: phagocytosis, pinocytosis and caveolae-dependent or clathrin-mediated endocytosis [28, 37, 38]. Hereinto, phagocytosis and pinocytosis usually occur in specialized immune system cells such as neutrophils and macrophages. In this work, the cell model is A549 human lung cancer cell and two major pathways have been focused on: caveolae-dependent endocytosis and clathrin-dependent endocytosis. To identify the internalization mechanism of HNTs, a series of inhibition studies were carried out. First, chlorpromazine (a drug to disrupt clathrin on the cell membrane) and filipin (a selective inhibitor of caveolae formation) were utilized to treat the cells. It was found that HNTs are predominantly localized to the cell boundaries and little intracellular fluorescence is observed. It indicates that the cellular uptake of

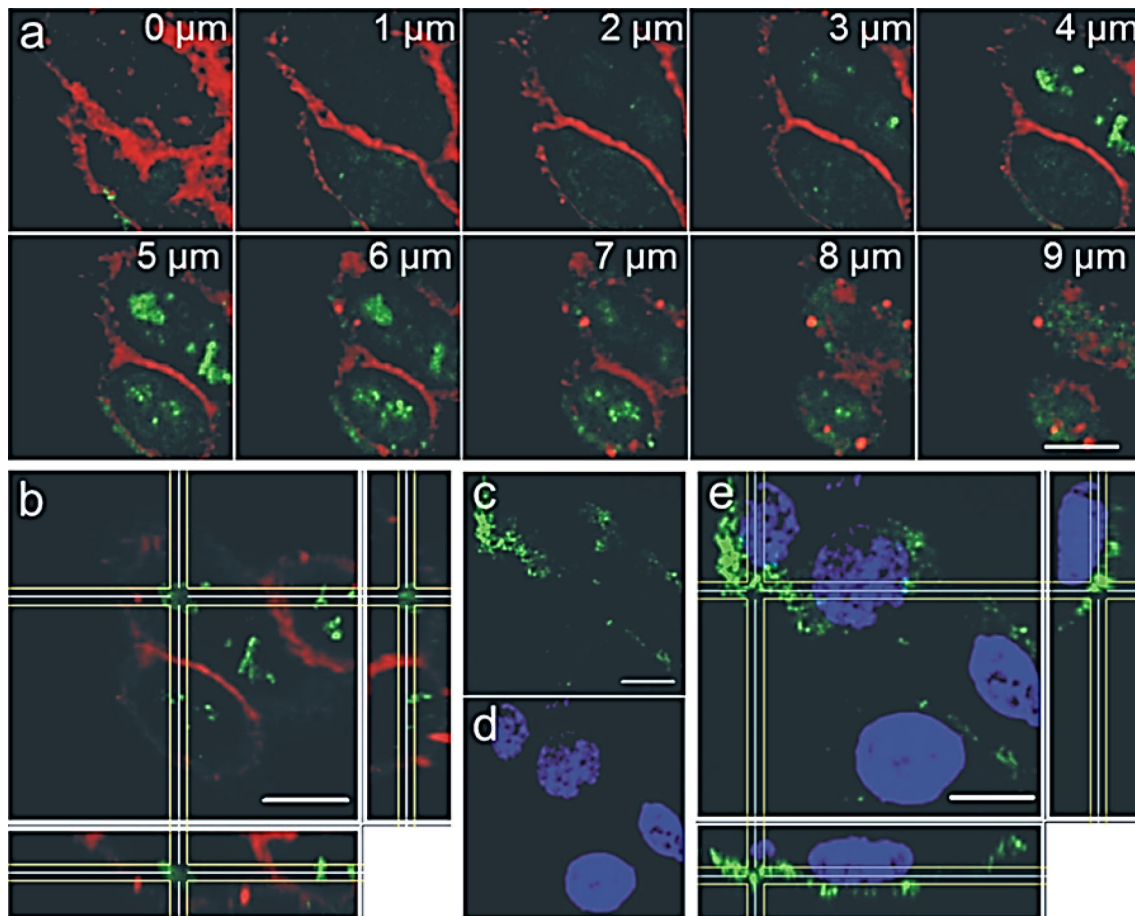


Figure 2 Distribution of FITC-labeled HNTs in living cells. **a** Gallery display of the intracellular distribution of FITC-labeled HNTs (green) enclosed in the cytomembrane (red), in accordance with the sequence from the bottom to the top of the cells. The Z-gap is 1 μm . **b** Snapshot of 3D display of cell profile with the

HNTs is significantly blocked (Fig. 4a, b). It may manifest that HNTs was mainly internalized via both clathrin- and caveolae-dependent endocytosis pathways.

What is the transport path of the halloysites after they enter the cells? To investigate transport pathway(s) of HNTs in living cells, the role of microtubule and actin filaments for HNTs transportation in living cells was tested. Nocodazole (a drug to disrupt microtubules) and cytochalasin D (a drug to induce depolymerization of F-actin) were preincubated with the cells, and the cellular uptake of HNTs was found to reduce dramatically. The results showed that microtubules and actin filaments had also participated in cellular trafficking of HNTs (Fig. 4c–d). By quantitative analysis, it is confirmed that the cellular uptake of HNTs reduced markedly at the presence of

internalization of labeled nanotubes. **c–e** Confocal microscope image of internalized HNTs in A549 cells. Sections of a Z-stack FITC fluorescence of HNTs (green) and Hoechst-fluorescence stained cells nuclei (blue) overlaid images. Scale bar: 10 μm .

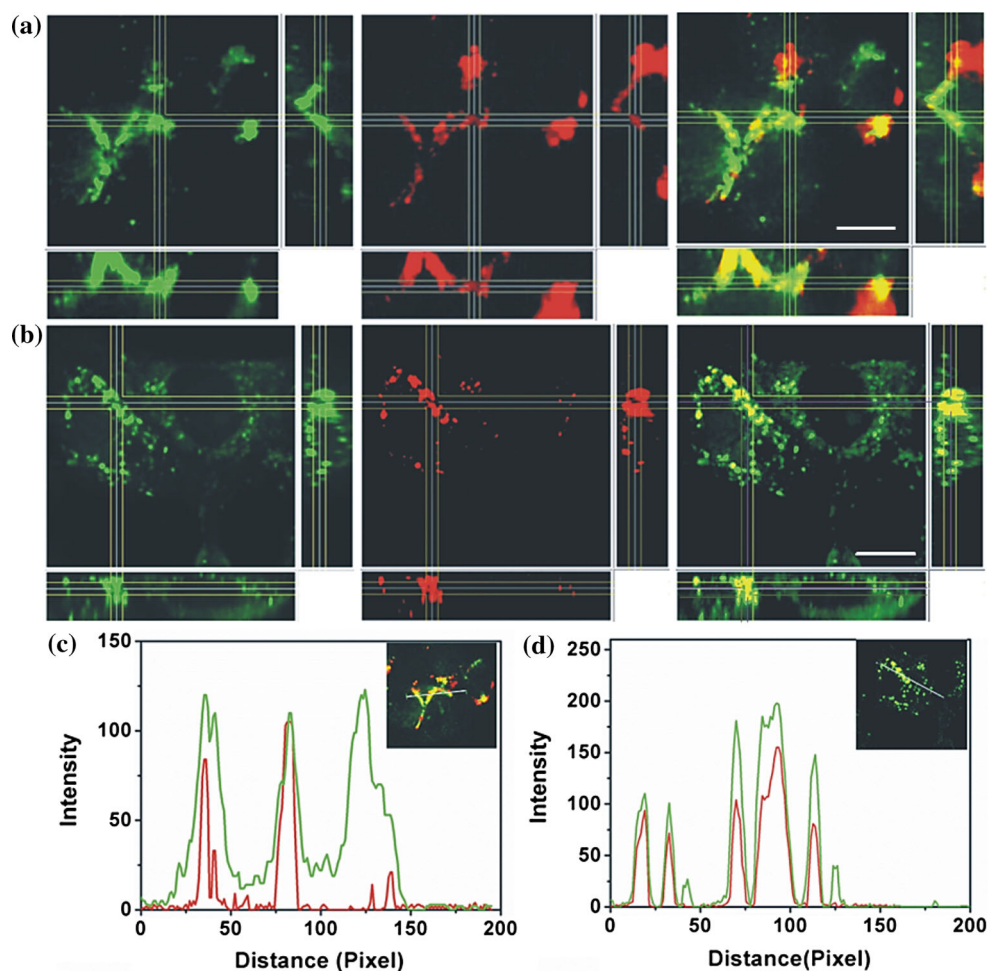
the four inhibitors. Overall, the HNTs were internalized into cells by both clathrin- and caveolae-dependent endocytosis and then transported by microtubules and actin filaments in living cells via Golgi apparatus and lysosome.

Cell cycle assay of drug-loaded HNTs

Cell cycle assays of both A549 cells and MRC-5 cells were performed using HNTs loaded with and without gemcitabine, and gemcitabine alone was administered as a control group. Generally, the decreased S phase arrest indicates the inhibition of cell division and restraining of cell growth [32, 33].

As shown in Fig. 5 and Tab. S1, the pristine HNTs almost have no effect on the cell cycle of A549 cells. Compared with pristine HNTs and gemcitabine

Figure 3 Tracking the endocytic process of halloysite nanotubes in live A549 cells: **a** Snapshots of FITC-labeled HNTs being trapped into Golgi apparatus. Colocalizations of FITC-labeled HNTs (green) and Golgi apparatus (red) resulted in yellow; **b** snapshots of FITC-labeled HNTs being trapped into lysosome. Colocalizations of FITC-labeled HNTs (green) and lysosome (red) resulted in yellow (scale bar: 10 μm); **c** line profile indicating the distribution of HNTs (green) and Golgi apparatus (red) signals on the line shown in the inset; and **d** line profile indicating the distribution of HNTs (green) and lysosome (red) signals on the line shown in the inset.

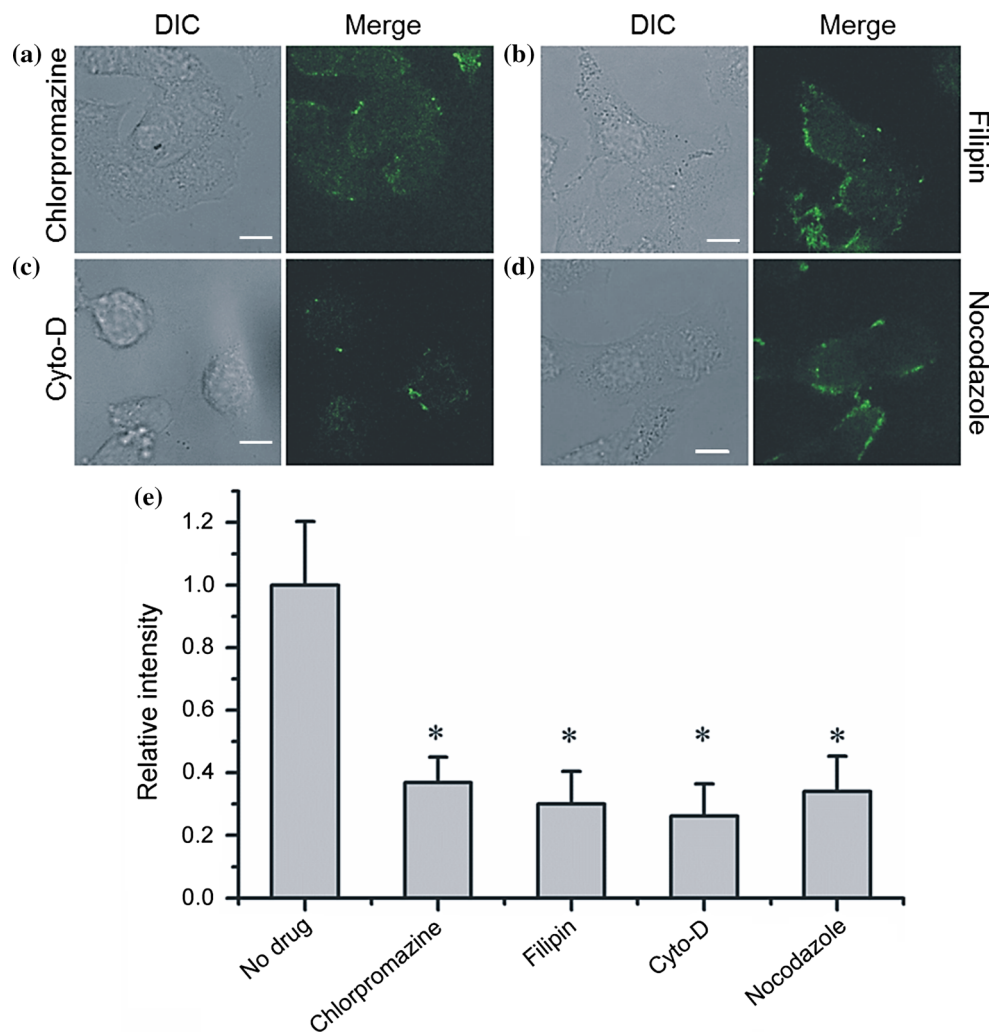


alone, gemcitabine-loaded HNTs revealed the strongest ability in decreasing S phase of A549 cells. These data may suggest that the decreased S phase for gemcitabine-loaded HNTs was a result of enhanced intracellular gemcitabine concentration, which further confirmed that HNTs contribute to the intracellular transportation of antitumor drug of A549 cells. In order to compare with normal cell lines, we selected MRC-5 as the control group and the affection of cell cycle of MRC-5 cells when co-cultured with HNTs, gemcitabine and HNTs +gemcitabine was detected (Fig. S4 and Tab. S2). Surprisingly, the S phase of MRC-5 in HNTs + Gemcitabine group displayed a significant increase compared to gemcitabine group.

Discussion

The cellular uptake of HNTs has aroused general concern among the researchers, who aimed to develop efficient tools for drug delivery in biomedical and pharmaceutical areas, and beyond. Although some early researches have claimed that HNTs could enter A549 cells and be aggregated inside cells with a time-dependent manner [34, 35], the detailed mechanisms about how HNTs are transported in living cells and which pathway is utilized by HNTs to internalize into the cells are still unclear. For the further development of HNTs as a drug carrier, it is imperative to perform in-depth studies in this direction to understand the specific uptake mechanism and transport pathway of HNTs. In this work, we studied the intracellular distributions of HNTs in living cells by fluorescence colocalization microscopy and detected the transport pathway of HNTs by inhibition studies. These allowed us to systematically

Figure 4 Inhibition of halloysite nanotubes endocytosis: the DIC image and fluorescence image of the cells pretreated by **a** chlorpromazine, **b** filipin, **c** Cyto-Dor, **d** nocodazole and **e** quantitative analysis of cellular uptake of halloysite nanotubes in the presence of various inhibitors. The column marked with (*) indicates that there is a significant statistical difference ($P < 0.01$) in fluorescence between the cells treated with the inhibitor and those without the treatment.



expound drug uptake mechanisms exploited by HNTs in living cells and to directly address how HNTs work as drug carriers in living cells. Our experimental findings showed that the transport process started from HNTs interacted with cell membrane, were internalized into cells by both clathrin- and caveolae-dependent endocytosis, then were transported by microtubules and actin filaments in the cytosol via Golgi apparatuses and lysosomes and finally aggregated in the perinuclear region of the living cells (Shown in Fig. 6).

The endocytosis-dependent process studies of carbon nanotubes, which also has a cylindrical nanostructure, were found to utilize only clathrin-mediated pathway to internalize into cells [36]. The difference in the internalization pathway of these two kinds of nanotubes may be because that cellular uptake of nanoparticles can be influenced by their properties, such as surface charge, composition and particle size

[37]. The predominant pathways of entry for nanoparticles could be shifted with the increase in particle size, because each endocytic pathway generates a distinctive size range of vesicles to trap internalized materials [37]. Therefore, the relatively wide range of sizes for HNTs may be the reason for why the internalization of HNTs is mediated by more than one cellular uptake pathways, not a single pathway. On the other hand, lysosomes act as the wastes disposal system of the cell and can cause a complete degradation of the exogenous materials, such as virus and carriers [38]. Thus, lysosome can help with the release of virus genome- and carrier-loaded drugs. Accordingly, our observation showed that the majority of HNTs is transported via lysosomes in the cytosol. This is indeed exciting, which may allow us to further optimize the drug-loaded HNTs properties to preferentially direct toward a preferred uptake route.

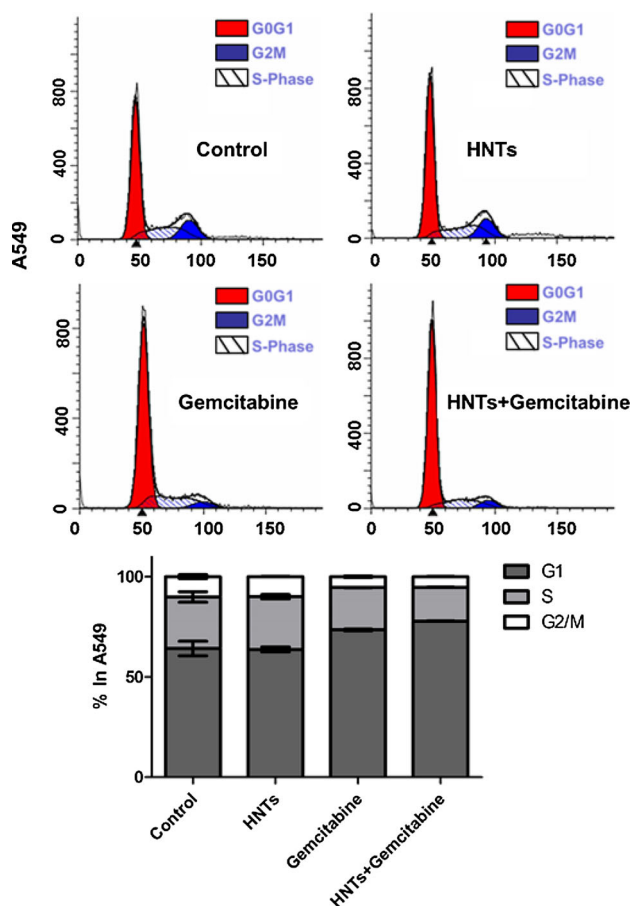


Figure 5 Cell cycle of A549 affected by HNTs (0.1 μ M), gemcitabine (0.1 μ M) and HNTs + gemcitabine (0.1 μ M) at 24 h after co-culture. A549 cells were stained with propidium iodide. The red area shows G1 phase, the white area shows S phase and the blue area shows G2/M phase. Quantitation of the fraction of cells in different cell cycle phases was done using GraphPad software. Bar diagram shows the % of cells present in different phases of cell cycle.

Gemcitabine is an antitumour drug and has been widely used in treating various kinds of cancers, such as non-small cell lung cancer, pancreatic cancer, bladder cancer and breast cancer. It is usually administered intravenously, which leads to its low selectivity and inefficient distribution [28]. However, HNTs have the capability of immobilizing drug molecules and transporting them through cell membranes in several different pathways, which may counteract the limitation of tradition administration of gemcitabine. Thus, we utilized HNTs to load gemcitabine and compared the drug effect on MRC-5 human lung cells and A549 human lung cancer cells. This allowed us to clarify the delivery ability of HNTs in living cells. Our results showed that gemcitabine-

loaded HNTs obviously inhibit the cell division and growth of A549 cells, which contribute to the delivery of gemcitabine in A549 cancer cells. In contrast, the S phase of MRC-5 cells was increased (Tab. S1). It may be because of lacking enhanced permeability and retention (EPR) effect for MRC-5 cells as a normal cell [39]. The EPR effect is the most important strategy to improve the delivery of therapeutic agents to tumors for anticancer drug development [40]. However, this EPR effect-driven drug delivery does not occur in normal tissues. EPR effect is applicable for any polymeric drugs (including nanoparticles, polymer micelles and liposomes) above 40 kDa or of the size of bacteria, which is apparently suitable for the anticancer drug-loaded HNTs [41]. Compared to A549 cells, MRC-5 cells are more difficult to uptake gemcitabine-loaded HNTs, thus significantly affect the controlled release of gemcitabine and reduce the huge effects of the anticancer drug in MRC-5 cells. These results imply that gemcitabine-loaded HNTs have distinguishable targeted characteristic into tumor cells.

The obvious advantages of HNTs, such as empty lumen, high adsorption ability, good biocompatibility, ease of dispersion within polymers, have obtained intense interest in the field of drug delivery. However, the size of HNTs in nature is uneven and in a wide range. Thus, the approaches should be developed to reduce the particle size of these halloysite nanotubes. In our study, we utilized a easy-performed separation strategy based on ultrasonic and centrifuge, by which we can obtain the relatively even distribution of the size of HNTs (225 ± 117 nm). This process can improve the efficiency of HNTs to enter the cells. We have examined the possibility of HNTs transportation into A549 cells through TEM as shown in Fig. S4 and provided the opportunity for further applications in vivo. Although HNTs are relatively difficult to degrade in vitro, our previous results showed that HNTs are degradable at a very low degradation rate under certain acidic environment. Strong acidic conditions accelerate the degradation rate of HNTs more significantly than weak alkaline conditions. Due to the distinction between in vitro and in vivo environments, the in vivo environment in tumor cells is more complicated and more acidic compared to normal cells. On the surface, the aluminosilicate chemical structure should be non-biodegradable, but the increase in specific surface area of HNTs nanoparticles can cause the

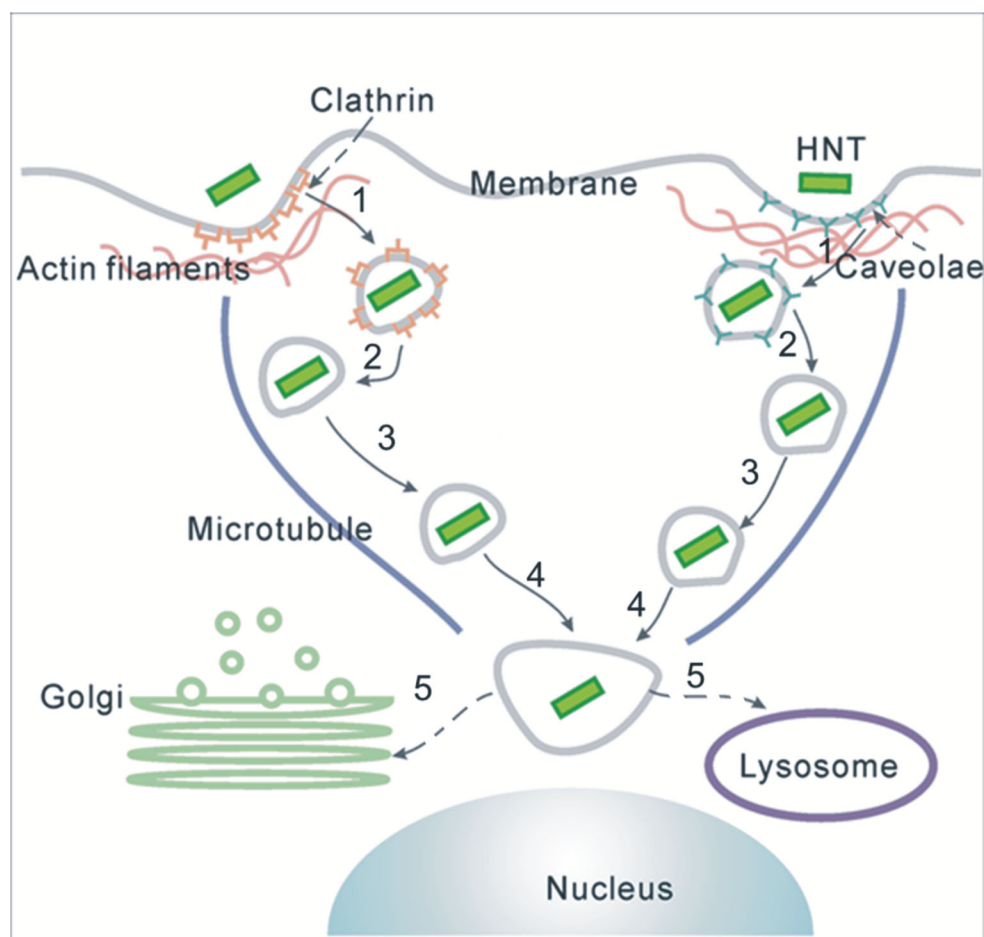


Figure 6 A predicted model for the transport of HNTs in living cells: The internalization pathway of HNTs includes five stages: HNTs being transported into cells near the cytomembrane via clathrin- or caveolae-dependent pathways (1), moving slowly

enhancement of ionic dissolution [42]. HNTs' biodegradability has not been probed clearly yet. However, it has been reported that HNTs reside among the safest nanoscale materials [43]. Thus, one may expect that chronic inflammatory reactions induced by HNTs in vivo do not occur. Meanwhile, since HNTs are transported into living cells by endocytosis, it is possible that HNTs may be excreted from cells by exocytosis within several hours. Furthermore, we will perform further investigation into the detailed mechanisms for intracellular delivery of HNTs in vivo.

along actin filaments (2), marching rapidly on microtubules (3), forming aggregation in the perinuclear region (4), and then being transported into Golgi apparatus or lysosome with a specific manner (5).

Conclusion

In general, the cellular uptake and transport mechanism of HNTs in live A549 cells have been studied. HNTs can enter into living cells readily and be aggregated in the perinuclear region of the living cells. Colocalization of HNTs with both Golgi apparatuses and lysosomes also demonstrates that HNTs could be transported via both of these organelles. Various endocytosis inhibition studies show that HNTs were internalized into cells by both clathrin- and caveolae-dependent endocytosis, and the cytoskeletons, including microtubules and actin filaments, are also involved in the transport pathway of HNTs in tumor cells. Flow cytometry results indicate that HNTs contribute to the intracellular delivery of gemcitabine, especially targeted for tumor cells. Such

conclusions of cellular transport pathways of HNTs may help in rational design of novel drug delivery systems and may also be of great value toward their applications in biomedicine and biotechnology.

Acknowledgements

This work was supported by China Scholarship Council (No.201208420587). The authors would also like to thank Prof. Daiwen Pang at Wuhan University for technical help with confocal microscopy and Dr. Matthew Glen and Dr. Lynne Waddington at CSIRO in Australia for technical assistance on SEM and TEM.

Compliance with ethical standards

Conflict of interest The authors declare no conflict of interests.

Electronic supplementary material: The online version of this article (<https://doi.org/10.1007/s10853-018-2775-5>) contains supplementary material, which is available to authorized users.

References

- [1] Shao W, Paul A, Zhao B, Lee C, Rodes L, Prakash S (2013) Carbon nanotube lipid drug approach for targeted delivery of a chemotherapy drug in a human breast cancer xenograft animal model. *Biomaterials* 34:10109–10119
- [2] Jia N, Lian Q, Shen H, Wang C, Li C, Yang Z (2007) Intracellular delivery of quantum dots tagged antisense oligodeoxynucleotides by functionalized multiwalled carbon nanotubes. *Nano Lett* 7:2976–2980
- [3] Xu ZP, Zeng QH, Lu GQ, Yu AB (2006) Inorganic nanoparticles as carriers for efficient cellular delivery. *Chem Eng Sci* 61:1027–1040
- [4] Wang F, Wang YC, Dou S, Xiong MH, Sun TM, Wang J (2011) Doxorubicin-tethered responsive gold nanoparticles facilitate intracellular drug delivery for overcoming multidrug resistance in cancer cells. *ACS Nano* 5:3679–3692
- [5] Pissuwan D, Niidome T, Cortie MB (2011) The forthcoming applications of gold nanoparticles in drug and gene delivery systems. *J Control Release* 149:65–71
- [6] Newman P, Minett A, Ellis-Behnke R et al (2013) Carbon nanotubes: their potential and pitfalls for bone tissue regeneration and engineering. *Nanomed Nanotechnol* 9:1139–1158
- [7] Levis S, Deasy P (2002) Characterisation of halloysite for use as a microtubular drug delivery system. *Int J Pharm* 243:125–134
- [8] Santos AC, Ferreira C, Veiga F, Ribeiro AJ, Panchal A, Lvov Y, Agarwal A (2018) Halloysite clay nanotubes for life sciences applications: from drug encapsulation to bioscaffold. *Adv Colloid Interface Sci.* <https://doi.org/10.1016/j.cis.2018.05.007>
- [9] Remškar M (2004) Inorganic nanotubes. *Adv Mater* 16:1497–1504
- [10] Joussein E, Petit S, Churchman J, Theng B, Righi D, Delvaux B (2005) Halloysite clay minerals—a review. *Clay Miner* 40:383–426
- [11] Kryuchkova M, Danilushkina A, Lvov YM et al (2016) Evaluation of toxicity of nanoclays and graphene oxide in vivo: a paramecium caudatum study. *Environ Sci Nano* 3:442–452
- [12] Lvov YM, DeVilliers MM, Fakhru'llin RF (2016) The application of halloysite tubule nanoclay in drug delivery. *Expert Opin Drug Deliv* 13:977–986
- [13] Vergaro V, Lvov YM, Leporatti S (2012) Halloysite clay nanotubes for resveratrol delivery to cancer cells. *Macromol Biosci* 12:1265–1271
- [14] Shi YF, Tian Z, Zhang Y, Shen HB et al (2011) Functionalized halloysite nanotube-based carrier for intracellular delivery of antisense oligonucleotides. *Nanoscale Res Lett* 6:1–7
- [15] Vergaro V, Abdullayev E, Lvov YM, Zeitoun A, Cingolani R et al (2010) Cytocompatibility and uptake of halloysite clay nanotubes. *Biomacromol* 11:820–826
- [16] Fix D, Andreeva DV, Lvov YM, Shchukin DG, Möhwald H (2009) Application of inhibitor-loaded halloysite nanotubes in active anti-corrosive coatings. *Adv Funct Mater* 19:1720–1727
- [17] Fakhru'llina GI, Akhatova FS, Lvov YM et al (2015) Toxicity of halloysite clay nanotubes in vivo: a caenorhabditis elegans study. *Environ Sci Nano* 2:54–59
- [18] Wu H, Shi Y, Huang C, Zhang Y, Wu J et al (2014) Multifunctional nanocarrier based on clay nanotubes for efficient intracellular siRNA delivery and gene silencing. *J Biomater Appl* 28:1180–1189
- [19] Dзамukova MR, Naumenko EA, Lvov YM et al (2015) Enzyme-activated intracellular drug delivery with tubule clay nanoformulation. *Sci Rep UK* 5:10560
- [20] Massaro M, Lazzara G, Milioto S, Noto R, Riela S (2017) Covalently modified halloysite clay nanotubes: synthesis, properties, biological and medical applications. *J Mater Chem B* 5(16):2867–2882

- [21] Verma NK, Moore E, Blau W, Volkov Y et al (2012) Cytotoxicity evaluation of nanoclays in human epithelial cell line A549 using high content screening and real-time impedance analysis. *J Nanopart Res* 14:1–11
- [22] Price R, Gaber BP, Lvov YM (2011) In-vitro release characteristics of tetracycline HCl, khellin and nicotinamide adenine dinucleotide from halloysite; a cylindrical mineral. *J Microencapsul* 18:713–722
- [23] Abdullayev E, Price R, Shchukin D, Lvov YM (2009) Halloysite tubes as nanocontainers for anticorrosion coating with benzotriazole. *ACS Appl Mater Interfaces* 1:1437–1443
- [24] Liu P, Zhao M (2009) Silver nanoparticle supported on halloysite nanotubes catalyzed reduction of 4-nitrophenol (4-NP). *Appl Surf Sci* 255:3989–3993
- [25] Veerabadran NG, Mongayt D, Torchilin V, Price R, Lvov YM (2009) Organized shells on clay nanotubes for controlled release of macromolecules. *Macromol Rapid Commun* 30:99–103
- [26] Serag MF, Kaji N, Venturelli E, Okamoto Y, Terasaka K et al (2011) Functional platform for controlled subcellular distribution of carbon nanotubes. *ACS Nano* 5:9264–9270
- [27] Khandare JJ, Jalota-Badhwar A, Satavalekar SD, Bhansali SG et al (2012) PEG-conjugated highly dispersive multi-functional magnetic multi-walled carbon nanotubes for cellular imaging. *Nanoscale* 4:837–844
- [28] Burris HA, Moore MJ, Andersen J et al (1997) Improvements in survival and clinical benefit with gemcitabine as first-line therapy for patients with advanced pancreas cancer: a randomized trial. *J Clin Oncol* 15:2403–2413
- [29] Martoni A, Marino A, Sperandi F et al (2005) Multicentre randomized phase III study comparing the same dose and schedule of cisplatin plus the same schedule of vinorelbine or gemcitabine in advanced non-small cell lung cancer. *Eur J Cancer* 41:81–92
- [30] Yah WO, Takahara A, Lvov YM (2012) Selective modification of halloysite lumen with octadecylphosphonic acid: new inorganic tubular micelle. *J Am Chem Soc* 134:1853–1859
- [31] Yuan P, Southon PD, Liu Z, Green ME, Hook JM, Antill SJ, Kepert CJ (2008) Functionalization of halloysite clay nanotubes by grafting with γ -aminopropyltriethoxysilane. *J Phys Chem C* 112:15742–15751
- [32] Li J, Wang R, Schweickert PG et al (2016) Plk1 Inhibition Enhances the Efficacy of Gemcitabine in Human Pancreatic Cancer. *Cell Cycle* 15:711–719
- [33] Zeng YC, Wu R, Xiao YP et al (2015) Radiation enhancing effects of sanazole and gemcitabine in hypoxic breast and cervical cancer cells in vitro. *Contemp Oncol* 19:236–240
- [34] Mailander V, Landfester K (2009) Interaction of nanoparticles with cells. *Biomacromol* 10:2379–2400
- [35] Conner SD, Schmid SL (2003) Regulated portals of entry into the cell. *Nature* 422:37–44
- [36] Kam NWS, Liu Z, Dai H (2006) Carbon nanotubes as intracellular transporters for proteins and DNA: an investigation of the uptake mechanism and pathway. *Angew Chem Int Ed* 118:591–595
- [37] Hillaireau H, Couvreur P (2009) Nanocarriers' entry into the cell: relevance to drug delivery. *Cell Mol Life Sci* 66:2873–2896
- [38] Liu SL, Zhang ZL, Tian ZQ et al (2011) Effectively and efficiently dissecting the infection of influenza virus by quantum-dot-based single-particle tracking. *ACS Nano* 6:141–150
- [39] Fang J, Nakamura H, Maeda H (2011) The EPR effect: unique features of tumor blood vessels for drug delivery, factors involved, and limitations and augmentation of the effect. *Adv Drug Deliv Rev* 63:136–151
- [40] Jin SE, Jin HE, Hong SS (2014) Targeted delivery system of nanobiomaterials in anticancer therapy: from cells to clinics. *Biomed Res Int* 2014:814208
- [41] Maeda H, Bharate GY, Daruwalla J (2009) Polymeric drugs for efficient tumor-targeted drug delivery based on EPR-effect. *Eur J Pharm Biopharm* 71:409–419
- [42] Watari F, Takashi N, Yokoyama A et al (2009) Material nanosizing effect on living organisms: non-specific, biointeractive, physical size effects. *J R Soc Interface* 6:S371–S388
- [43] Kryuchkova M, Danilushkina A, Lvov Y, Fakhruллин R (2016) Evaluation of toxicity of nanoclays and graphene oxide in vivo: a *Paramecium caudatum* study. *Environ Sci Nano* 3(2):442–452